Theory of the bimetallic interface

J. Ferrante
National Aeronautics and Space Administration, Lewis Research Center, Cleveland, Ohio 44135

J. R. Smith
Physics Department, General Motors Research Laboratories, Warren, Michigan 48090-9055
(Received 8 March 1984)

The self-consistent electronic structure and adhesive energetics are computed for contacts between all combinations of Al(111), Zn(0001), Mg(0001), and Na(110). The electronic structure is quite different from that of contacts between identical metals, with large electronic potential barriers appearing even at the smallest separations. Charge transfer and/or rearrangement distributions are plotted for various contact separations. These density differences lead to potential differences, or changes in the electronic potential distributions in the interfaces due to charge transfer and/or rearrangement. They have little relation to the contact potential, and vary rapidly with contact interfacial separation. The kinetic energy initiates the bond, while the exchange-correlation energy is the dominant contributor to the strength of the adhesive bond. The range of strong bonding is about 0.2 nm. Electronic barrier heights saturate more slowly with contact separation. One can expect metallic transfer for the contacts involving Na, but it is less likely for the others. A universal adhesive energy relation was found to accurately describe the energetics of all ten bimetallic interfaces considered here. Because of this universality, one can expect to determine the energetics of other bimetallic interfaces via a simple scaling of the universal relation. A close relationship is revealed between diatomic molecular bonds and bonds across a bimetallic interface.

I. INTRODUCTION

Because of the strong interactions occurring between metals in intimate contact, there can be significant changes in the electronic structure as a function of separation between the surfaces. We have studied[1] this phenomenon for the case in which the two metals are identical. When the two metals are different, charge transfer can occur with the formation of contact potentials. Unlike identical-metal contacts, this charge transfer can cause significant electronic barriers in the interface even at the smallest separations. The interface electronic structure influences electronic contact behavior. Further, metallic transfer is found when the bond between the two metals is stronger than either of the parent metals. The strong adhesive bonds formed between metals in intimate contact play an important role[2] in the deposition of metal films, grain-boundary energetics, friction and wear, electrical contacts, and fracture.

Earlier calculations on the bimetallic interface were done by Bennett and Duke[3] and by the authors.[4] The work of Ref. 3 was not fully self-consistent and binding or adhesive energies were not computed. In Ref. 4 binding energies were computed as a function of separation between interfaces, but the approximation of simple overlap of the solid-vacuum electron distributions was made.

In the following we report the first fully self-consistent calculations of adhesive energies and electronic structure for bimetallic interfaces. All combinations of Al(111), Zn(0001), Mg(0001), and Na(110) are treated. The results for adhesive energetics led to the discovery of a universal energy relation[5] in terms of which the energetics of bimetallic interfaces can be described in considerable generality. Subsequently, it was found that this universality extended to chemisorption,[6] cohesion, diatomic-molecule energetics, and even to nuclear matter.[7]

II. THEORETICAL METHODS

The calculational formalism and methods used for obtaining self-consistent interface electronic structure will now be presented. The discussion of these methods, while apparently similar, will differ essentially from that of Ref. 1 since in this case we will be considering dissimilar metals in contact.

The adhesive interaction energy E_{ad} between two metal surfaces is a function of the distance between the two surfaces, a (see Fig. 1). E_{ad} is defined as the negative of the amount of work necessary to increase the separation from a to ∞ divided by twice the cross-sectional area A. Thus

$$E_{ad}=[E(a)-E(\infty)]/2A \ , \tag{1}$$

where E is the total energy. For identical metals, E_{ad} is the negative of the surface energy when a is at the energy minimum.

The total energy is given by[8,9] (atomic units are used throughout unless otherwise specified)

$$E\{n(\vec{r})\}=\int v(\vec{r})n(\vec{r})d\vec{r}+\tfrac{1}{2}\sum_{\substack{i,j\\(i\neq j)}}\frac{z_i z_j}{R_{ij}}+F\{n(\vec{r})\} \ , \tag{2}$$

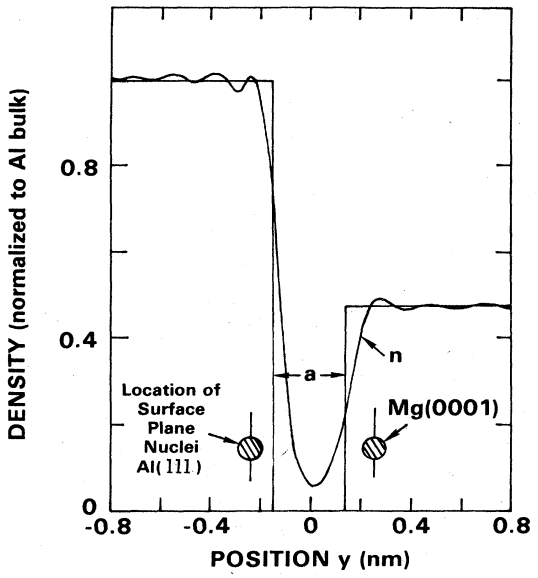

FIG. 1. Electron number density n and jellium-ion charge density n_+ for an Al-Mg contact. When $a=0.0$, the distance between Mg and Al atomic planes is $(d_{\mathrm{Al}}+d_{\mathrm{Mg}})/2$, where d_{Al} and d_{Mg} are the respective bulk interplanar spacings.

where

$$F\{n(\vec{r})\}=T_s\{n(\vec{r})\}+\tfrac{1}{2}\int\int\frac{n(\vec{r})n(\vec{r}')}{|\vec{r}-\vec{r}|}d\vec{r}\,d\vec{r}'+E_{\mathrm{xc}}\{n(\vec{r})\}\ , \tag{3}$$

$v(\vec{r})$ is the ionic potential, and $n(\vec{r})$ is the electron number density. The first two terms in Eq. (2) are the electron-ion and ion-ion interaction energies, respectively. The ionic charge is z and R_{ij} is the distance between ion-core nuclei (there is no ion-core overlap in the systems considered here). $T_s\{n(\vec{r})\}$ is the kinetic energy of a system of noninteracting electrons with the same density $n(\vec{r})$, the next term is the classical electron-electron interaction energy, and E_{xc} is the exchange-correlation energy.

The metals Zn, Mg, Al, and Na are well described by the jellium model (Fig. 1) in the zeroth-order approximation. That is, the difference between the total pseudopotential and the potential due to the jellium for each metal is small for the closest-packed plane. Thus for a given separation a, one obtains E to a first-order perturbation approximation as

$$E\{n(\vec{r})\}=A\int v_J(y,a)n(y,a)dy+\tfrac{1}{2}\sum_j\sum_{i\,(\neq j)}\frac{z_iz_j}{R_{ij}}+F\{n(y,a)\}+A\int\delta v(y,a)n(y,a)dy\ , \tag{4}$$

where v_J is the potential produced by the jellium, y is the direction normal to the surfaces, and δv is the average, over planes parallel to the surface, of the difference in potential due to an array of pseudopotentials and that from a jellium surface. As in our calculations[1] for cases when the two metals are identical, for the pseudopotential we chose that due to Ashcroft.[10] The Schrödinger equation is of the form

$$\left[-\frac{1}{2}\frac{d^2}{dy^2}+v_{\mathrm{eff}}(n;y)\right]\psi_k^{(i)}(y)=\tfrac{1}{2}(k^2-k_F^2)\psi_k^{(i)}(y)\ , \tag{5}$$

where

$$v_{\mathrm{eff}}(n;y)=\phi(y,a)+\frac{\delta E_{\mathrm{xc}}\{n(y,a)\}}{\delta n(y,a)} \tag{6}$$

and where k is the Bloch vector component in the y direction.

In order to calculate the wave functions, we define two regions in energy space. Refer to Fig. 2, where our notation is defined for the example case of Al(111) on the left-hand side and Mg(0001) on the right-hand side. The first region (region 1), is for energies below the bottom of the band of smaller width, which in this case is below the bottom of the Mg band. There is only one linearly independent solution in this case, with asymptotic forms

$$\psi_{k_L}(y)=(2\pi k_L)^{-1/2}(e^{ik_Ly}+u_{11}e^{-ik_Ly}),\quad y\to-\infty$$
$$\psi_{k_R}(y)=(2\pi k_R)^{-1/2}u_{21}e^{-k_Ry},\quad y\to\infty \tag{7a}$$

where $k_R\equiv(k_{FD}^2-k_L^2)^{1/2}$.

The second region (region 2) is above the bottom of the band of smaller width (which is hereafter assumed to belong to the metal on the right-hand side), and below the Fermi level E_F. The two linearly independent, degenerate solutions have asymptotic forms as

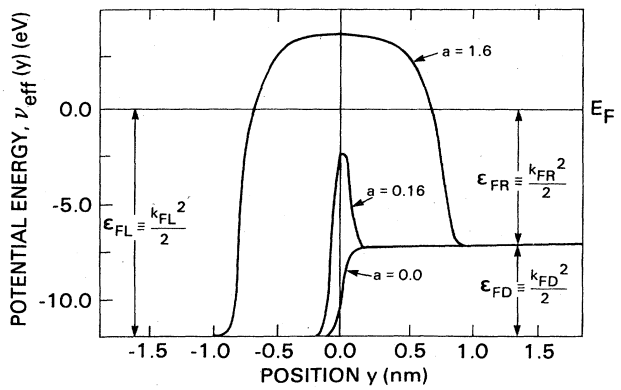

FIG. 2. Electron potential energy $v_{\mathrm{eff}}(y)$ versus position for an Al-Mg contact (Al is on the left-hand side), at separations of 0, 0.16, and 1.6 nm.

$$\psi^{(1)}_{k_L}(y)=(2\pi k_L)^{-1/2}(e^{ik_L y}+u_{11}e^{-ik_L y}),\quad y\to-\infty$$
$$\psi^{(1)}_{k_R}(y)=(2\pi k_R)^{-1/2}u_{21}e^{ik_R y},\quad y\to\infty \tag{7b}$$
$$\psi^{(2)}_{k_L}(y)=(2\pi k_L)^{-1/2}u_{12}e^{-ik_L y},\quad y\to-\infty$$
$$\psi^{(2)}_{k_R}(y)=(2\pi k_R)^{-1/2}(e^{-ik_R y}+u_{22}e^{ik_R y}),\quad y\to\infty\ .$$

From the fact that the Wronskian is independent of y we find that the wave functions $\psi^{(i)}(y)$ are orthogonal. The expressions in Eq. (7b) satisfy continuum normalization conditions. For Eq. (7b) we then find that the collision matrix $\underline{u}$ is unitary, where

$$\underline{u}=\begin{bmatrix} u_{11} & u_{12} \\ u_{21} & u_{22} \end{bmatrix} \tag{8}$$

The electron number densities from the two regions are thus given by

$$n_1(y,a)=\frac{2s+1}{2\pi}\int_0^{\epsilon_{FD}} d\epsilon(\epsilon_{FL}-\epsilon)\,|\,\psi_\epsilon(y)\,|^2\ , \tag{9}$$

$$n_2(y,a)=\frac{2s+1}{2\pi}\sum_i\int_{\epsilon_{FD}}^{\epsilon_{FL}} d\epsilon(\epsilon_{FL}-\epsilon)\,|\,\psi^{(i)}_\epsilon(y)\,|^2\ , \tag{10}$$

where continuum normalization was used for the wave functions of Eqs. (7a) and (7b) and $\epsilon\equiv k_L^2/2$.

The electron density is then

$$n(y,a)=n_1(y,a)+n_2(y,a)\ . \tag{11}$$

Equations (5)—(11) must be solved self-consistently with Poisson's equation

$$\frac{d^2\phi(y,a)}{dy^2}=-4\pi[n(y,a)-n_+(y)]\ . \tag{12}$$

$\phi(y,a)$ is the electrostatic potential; $n_+(y)$ is the jellium density (Fig. 1).

It is useful to combine the first two terms of Eq. (4) along with the classical electron-electron interaction term of $F\{n(y,a)\}$ as follows:

$$-\tfrac{1}{2}A\int\rho(y,a)\phi(y,a)dy+W_{\rm int}(a)\ , \tag{13}$$

where $\rho(y,a)$ is the net charge density of the zeroth-order jellium solution. $W_{\rm int}(a)$ is the exact difference between the ion-ion and the jellium-jellium interaction and is negligible unless the facing planes are in registry, i.e., commensurate.[4] In this calculation we assume for definiteness incommensurate adhesion [$W_{\rm int}(a)=0$], unless the two metals are identical, since registry is not obtained with dissimilar metals in contact without corresponding loss of energy due to strains. This strain energy can be evaluated in specific cases.[11] Zn and Al have Wigner-Seitz radii of 3.0 and 2.9 a.u., respectively. Mg and Na have radii of 3.3 and 3.9 a.u., respectively. Thus on that basis alone, Zn and Al would most easily distort into commensuration. Such distortion is ignored in this first investigation of the bimetallic interface.

The exchange-correlation energy $E_{\rm xc}$ is written in the local-density approximation,

$$E_{\rm xc}\{n(\vec{r})\}=\int n(\vec{r})\epsilon_{\rm xc}(n(\vec{r}))d\vec{r}\ , \tag{14}$$

where $\epsilon_{\rm xc}(n(\vec{r}))$ is the exchange-correlation energy of a uniform electron gas of number density $n(\vec{r})$. We use Wigner's interpolation formula for the correlation energy and the Kohn-Sham exchange energy.[9]

The specification of the kinetic-energy functional of Eq. (3),

$$T_s\{n(y,a)\}=A\int t_s\{n(y,a)\}dy\ , \tag{15}$$

now remains, where

$$t_s\{n(y,a)\}=\sum_{i=1}^{2}\sum_{\substack{k_L,k_x,k_z\\(\rm occ)}}(k_L^2+k_x^2+k_z^2)\,|\,\psi^{(i)}_{k_L}(y)\,|^2$$
$$+[v_{\rm eff}(n;-\infty)-v_{\rm eff}(n;y)]n(y,a)\ . \tag{16}$$

The sum is over all occupied states. The summation index i again refers to degenerate wave functions as in Eq. (5). In Appendix B of Ref. 1, an expression for $T_s\{n(y,a)\}-T_s\{n(y,0)\}$ is presented which is based on kinetic-energy densities in the interface region. We find this approach more natural for our problem, as it is the interface region in which the large changes in kinetic-energy density occur upon adhesion.

The Hamiltonian is now completely specified. In the remainder of this section we will elucidate some of the techniques used to deal with Eqs. (5) and (12).

The numerical integration of the Schrödinger equation and Poisson's equation was done over a slab width (distance between the bulk matching point in one metal to the corresponding point in the other metal) of $40+a$ a.u. (a is the distance between jellium surfaces). The solution to the Schrödinger equation proceeded by breaking the k space into two regions, below the conduction band in the less dense metal and above it. Below the conduction band the integration was started by assuming $\psi=e^{-k_R y}$ deep in the less dense metal and matching to $B(e^{ik_L y}+u_{11}e^{-ik_L y})$ deep in the more dense metal [see Eq. (7a)]. Above the conduction-band bottom, the doubly degenerate solutions were started by assuming from $\psi=e^{\pm iky}$ deep in the left or right half-space and matching to $C(e^{\pm iky}+ue^{\mp iky})$ deep in the other half-space. The solutions were then normalized to the form given in Eq. (7). The potential was required to match the bulk potential at the matching points.

The calculation was initiated from a trial potential generated by splicing together at the midpoint potentials from same-metal calculations. The solution proceeded by integration in which the potential for the input of an iteration loop was obtained from a linear combination of input and output potentials. The system of equations is highly unstable, and, consequently, only a small percentage of the output is included in the input. The percentage is periodically increased to speed up convergence and then decreased to damp out the instabilities created by the higher convergence factor. The calculations were stopped when the differences between input and output were less than 10 meV everywhere. As a further check on self-consistency, a comparison was made with an extension of the Budd-Vannimenus sum rule[12] for bimetallic interfaces

TABLE I. Raykov self-consistency check for Al-Zn. From the exact expression for the bulk pressure difference, we have 1.1932×10^{-3} a.u. for all values of separation.

Separation (a.u.)	Bulk pressure difference between Al and Zn from computed surface potentials (10^{-3} a.u.)
0.0	1.1951
0.25	1.1953
0.5	1.1926
0.75	1.195
1.0	1.1952
1.5	1.1966
2.0	1.1960
2.5	1.1932
3.0	1.1912
4.0	1.201
5.0	1.1936
10.0	1.1919
15.0	1.1946
30.0	1.1956

performed by Raykov.[13] Raykov showed that the difference in bulk electronic pressures can be written in terms of the electrostatic potentials at the two jellium surfaces. A typical result for all metal combinations is shown in Table I for an Al-Zn interface.

III. RESULTS AND DISCUSSION

Before proceeding with the results of the different-metal calculations, we present a result which extends our previous same-metal calculations and acts as a further check on those results. In Ref. 1 the calculations were stopped at a separation of 15 a.u. since the binding energy had essentially saturated at a separation of 10 a.u. The potential barrier height had not saturated at 15 a.u., and the bare metal work function differed substantially from our 15-a.u. value. In the bimetallic case we are interested in barrier heights at large separations in order to compute contact potentials. Consequently, the calculations were extended to a 30-a.u. separation. The results for the same-metal barrier height (maximum in potential minus bulk potential) versus separation for the four contacts are shown in Fig. 3. As can be seen, the barrier in the present calculation approaches the Lang-Kohn[14] solid-vacuum interface values asymptotically, as they should.

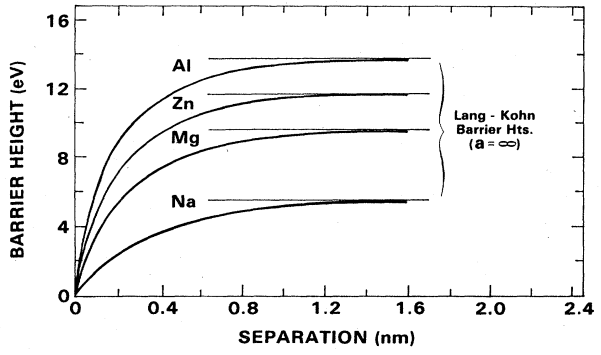

FIG. 3. Electronic barrier heights as a function of separation in the following contacts: Al-Al, Zn-Zn, Mg-Mg, and Na-Na.

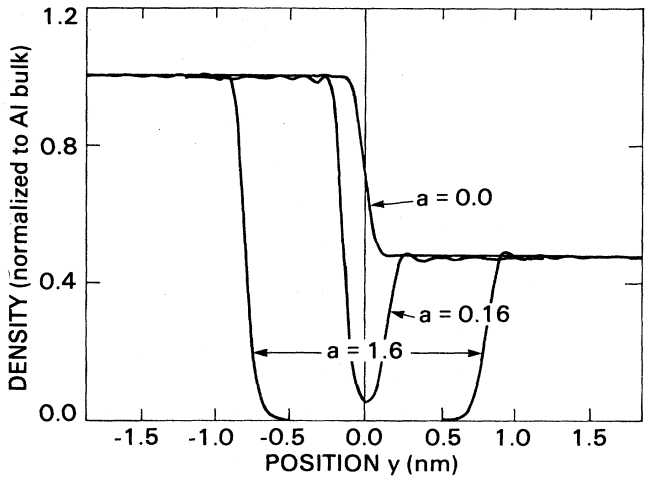

FIG. 4. Electron density versus position for an Al-Mg contact (Al is on the left-hand side), for separations of 0, 0.16, and 1.6 nm.

Figure 4 shows the electronic charge distributions in the interface between Al and Mg at separations $a = 0$, 3, and 30 a.u. (0, 0.16, and 1.6 nm). It is typical and exhibits the large differences in bulk electron densities in the metals considered. Because of these large differences, there is a strong gradient in the charge distribution through the interface even at the smallest separations. This and the net charge transfer leading to a contact potential are the most obvious differences between a bimetallic junction and a junction between identical metals.

For example, even for $a = 0$ the Al-Mg junction (see Fig. 2) exhibits a significant electronic barrier height in the interface, 4.6 eV. For the identical-metal junctions the barrier is zero at $a = 0$ (see Fig. 3). As with junctions between identical metals, the charge and potential distribution gradients increase with a, as do the Friedel oscillation amplitudes (see Figs. 2 and 4). The interface barriers, i.e.,

TABLE II. Comparison of interface barriers at large separation with work functions.

Interface barrier (eV) $a = 1.59$ nm		Work functions[a] (eV)	
Al-Al	3.79	Al	3.87
Zn-Zn	3.76	Zn	3.80
Mg-Mg	3.62	Mg	3.66
Na-Na	3.01	Na	3.06
Al-Zn	3.76		
Al-Mg	3.69		
Al-Na	3.42		
Zn-Mg	3.69		
Zn-Na	3.41		
Mg-Na	3.32		

[a]See Ref. 14.

the difference between the highest point in the potential distribution and the Fermi level, varies rapidly with a as exemplified in Fig. 2. In Table II these barriers are listed for an $a=30$ a.u. $=1.59$ nm. For comparison, the solid-vacuum work functions are given. The same-metal results appear to approach the work functions as expected (see also Fig. 3). The bimetallic interface barriers are intermediate between the work functions of the two metals. The electronic barrier heights (and shapes) really have little relation to the contact potential. Unlike the barrier heights, the contact potential is independent of separation a, in principle, and is typically much smaller than the barrier heights.

Our earlier[4] simple-overlap results by constraint did not allow for charge rearrangement and resulting contact potentials. In Fig. 5 we plot the self-consistent electron-density distribution in an Al-Na interface at zero separation ($a=0.0$) as the dashed curve. The solid curve is the result of adding the solid-vacuum densities for Al and Na, respectively (simple overlap). One can see that these two curves are indeed very close, and for some quantities—like perhaps total energies—simple overlap might be a reasonable approximation for the electron densities. Figure 6(a) shows the self-consistent densities minus the simple-overlap densities for $a=0.0$. It suggests that there is a net charge transfer from the Na (the metal on the right-hand side) to the Al (the metal on the left-hand side). This is consistent with the work function of Na being smaller than that of Al (Table II).

In Fig. 6(b) we have plotted the self-consistent or relaxed potential minus the simple-overlap potential for the Al-Na interface at $a=0.0$. Note the charge transfer leads to a contact potential ΔV of 0.81 eV, where

$$\Delta V=-4\pi\int_{-\infty}^{\infty} y\,\delta n(y)\,dy\ , \tag{17}$$

and where $\delta n(y)$ is the density difference plotted in Fig. 6(a).

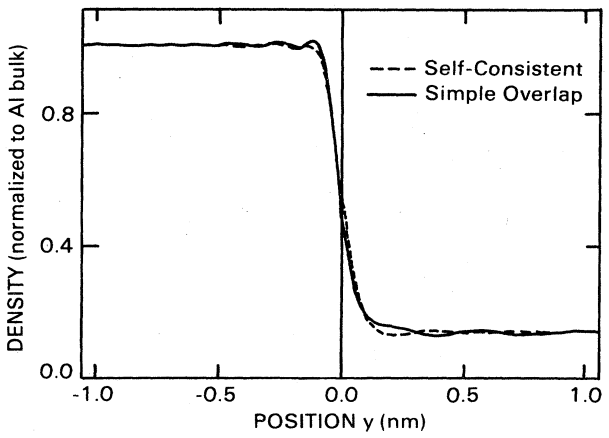

FIG. 5. Electron density distributions in the Al-Na interface at zero separation ($a=0.0$). The dashed curve is the fully-self-consistent result, while the solid curve results from a simple overlap of the solid-vacuum results for each of the two metals.

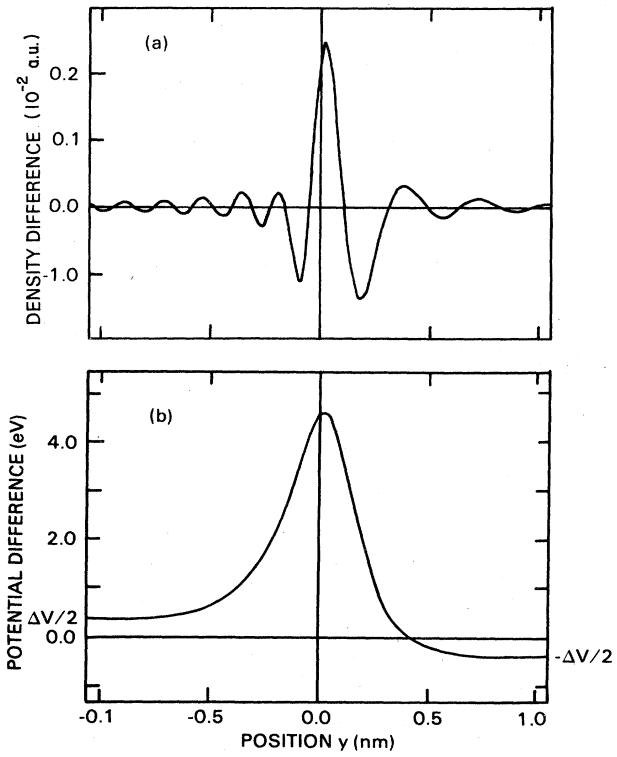

FIG. 6. (a) Self-consistent electron densities, $n(y,a)$, minus overlapped solid-vacuum electron densities for $a=0.0$ in an Al-Na contact (Al on the left-hand side). This density difference plot shows the charge rearrangement due to interaction between the Al and Na surfaces. (b) Self-consistent electron potentials $v_{\text{eff}}(n;y)$ minus overlapped solid-vacuum electron potentials for $a=0.0$ in an Al-Na contact. The contact potential ΔV is given by Eq. (17), where $\delta n(y)$ in that equation is plotted in (a).

However, the potential difference or transfer potential actually peaks 4.2 eV higher than the contact potential. Thus the commonly used contact potential really does not adequately describe what takes place in the interface. Figure 7 shows the corresponding results for the Al-Na interface at $a=30.0$ a.u. Figure 7(a) shows clearly that electrons are being transferred from the Na to the Al. Note the change of scale relative to Fig. 6(a). The charge-density difference must diminish in amplitude as a increases, so that the contact potential ΔV is independent of a. Note also from Fig. 7(b) that the contact potential ΔV is again 0.81 eV, as it must be, but the transfer potential has a markedly different shape than it had at $a=0.0$. At $a=30.0$ a.u., the peak in the transfer potential is quite close to the contact potential. The potential shape between the two metals is nearly linear, as one would expect at large separations since then each surface has a net charge with a large vacuum region between metals which has negligible charge in it.

Figure 8 exhibits the adhesive binding energies as a function of separation in bimetallic contacts made between all combinations of the four metals. The results from our previous work on same-metal contacts is includ-

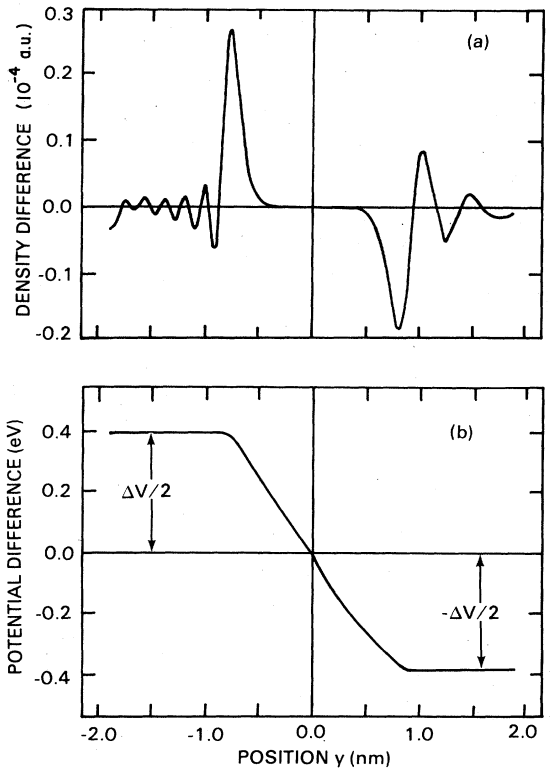

FIG. 7. (a) Self-consistent electron densities $n(y,a)$ minus overlapped solid-vacuum densities $n(y,a)$ for $a=1.59$ nm in an Al-Na contact, Al on the left-hand side. This shows clearly that electrons are transferred from the Na to the Al. (b) Self-consistent electron potentials $v_{\text{eff}}(n;y)$ minus overlapped solid-vacuum electron potentials for $a=1.59$ nm in an Al-Na contact. ΔV is the contact potential resulting from the charge transfer shown in (a).

ed in Fig. 9. As with identical-metal contacts, the range of strong bonding is about 0.2 nm for bimetallic contacts. It is clear that there is a considerable variation in shape and depth of these curves.

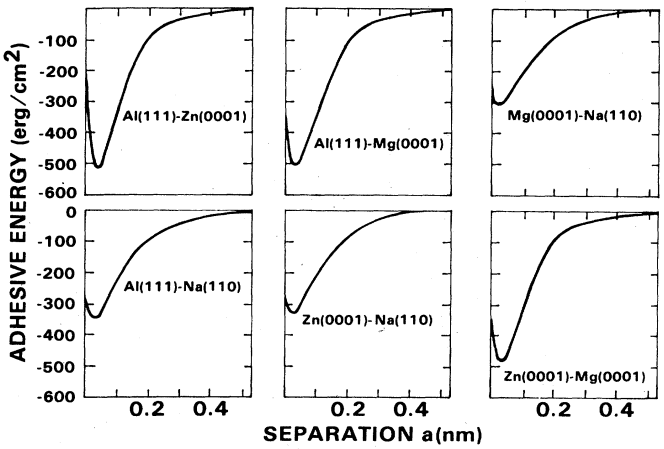

FIG. 8. Adhesive binding energy versus separation a. Incommensurate adhesion is assumed ($W_{\text{int}}=0$).

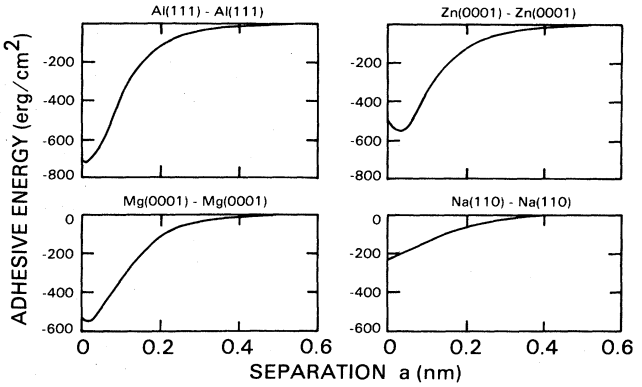

FIG. 9. Adhesive binding energy versus separation a. Commensurate adhesion is assumed ($W_{\text{int}}\neq 0$).

In Fig. 10 we show a breakdown of the components of the total energy as a function of separation for an Al-Mg contact. Note that the kinetic energy initiates the bond. In analogy with the molecular bond,[15] smoothing of the wave functions in the bonding region lowers the kinetic energy with respect to infinite separation. The electrostatic energy is repulsive at large separations, but becomes attractive at smaller separations. The dominant binding term is the exchange-correlation energy, as is evident from Fig. 10. The dominant repulsive term is the kinetic energy at small separation.

It is interesting to compare the binding energies at the minima with those of the identical-metal contacts (see Figs. 8 and 9). For incommensurate adhesion ($W_{\text{int}}=0$), Table III indicates that the metal binding energies fall into two groups: those involving Na and those not involving Na. The combination involving only Al, Zn, and Mg all have binding energies around 500 ergs/cm^2. Those bimetallic contacts involving Na all have binding energies around 300 ergs/cm^2. Perhaps this follows from the results for incommensurate ($W_{\text{int}}=0$) contacts between

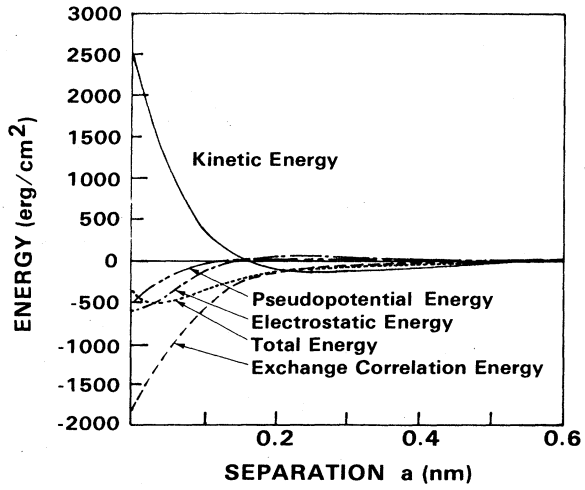

FIG. 10. Self-consistent energy components of the binding energy for an Al(111)-Mg(0001) contact.

TABLE III. Binding energy comparison. All energy values taken from the minimum in the adhesive energy plots (see Figs. 8 and 9).

Metal combination	Binding energy (ergs/cm^2) $W_{int}=0$	Perfect registry
Al(111)-Al(111)	490	715
Zn(0001)-Zn(0001)	505	545
Mg(0001)-Mg(0001)	460	550
Na(110)-Na(110)	195	230
Al(111)-Zn(0001)	520	
Al(111)-Mg(0001)	505	
Al(111)-Na(110)	345	
Zn(0001)-Mg(0001)	490	
Zn(0001)-Na(110)	325	
Mg(0001)-Na(110)	310	

identical metals in which, as Table III shows, the Al, Zn, and Mg contacts have nearly the same binding energies which are about 300 ergs/cm^2 above that for the Na contact.

A topic of interest is whether the interface is stronger or weaker than the bulk of one of the metals. If the interface were stronger, then there would be a possibility of transfer of one metal onto the other as a result of an adhesive bond. Since the bulk of the parent metals is in perfect registry, one needs to compare the perfect registry results with the incommensurate bimetallic results. One can see that only the bimetallic junctions involving Na could be expected to exhibit transfer. The Al-Zn junction strength is close to, but less than the Zn-Zn strength. One should bear in mind that defect structures and true contact-area considerations may be important to transfer and are not included in this work.

We wish now to look for systematics in the adhesive energy relations of Figs. 8 and 9. There are quite a variety of shapes and amplitudes there. We have found,[7] however, that these 10 relations can be scaled quite accurately into a single, universal relation; as shown in Fig. 11. The deviation of the separation a from the equilibrium value a_m is scaled as

$$a^* \equiv (a - a_m)/l \tag{18}$$

and the amplitude $E_{ad}(a)$ is scaled as

$$E^*_{ad}(a) \equiv E_{ad}(a)/\Delta E \ , \tag{19}$$

where ΔE is the magnitude of $E_{ad}(a)$ at the respective minima of the curves in Figs. 8 and 9, and where

$$l \equiv \left[\Delta E \left[\frac{d^2 E_{ad}(a)}{da^2} \right]^{-1}_{a_m} \right]^{1/2} , \tag{20}$$

so that

$$\left[\frac{d^2 E^*_{ad}(a^*)}{da^{*2}} \right]_0 = 1 \ . \tag{21}$$

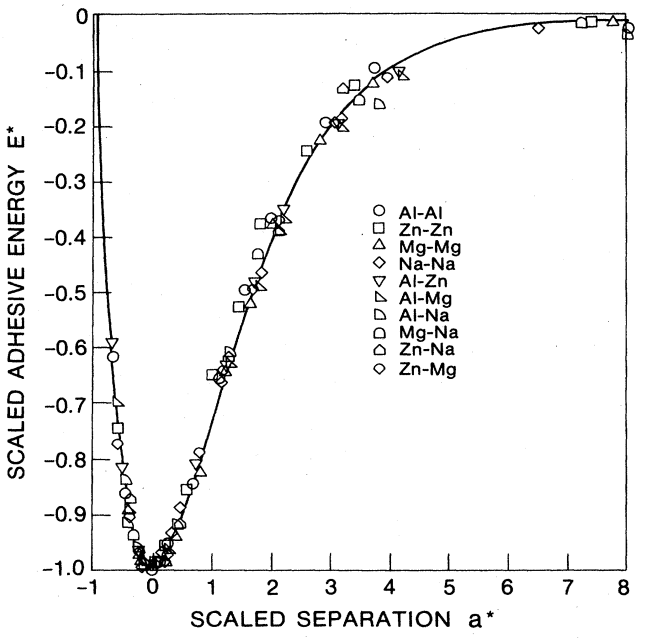

FIG. 11. Adhesive energy results from Figs. 8 and 9 scaled as described in the text [see Eqs. (18)—(21)].

One can see from Fig. 11 that the results for all 10 bimetallic contacts lie very close to the universal curve. This is true even though the bulk metallic densities in the various metals vary by a factor of 8. Thus, the extensive numerical calculations described earlier have led to the discovery of very simple relationships [Eqs. (18)—(20)], governing the energetics of bimetallic interfaces. The scaling length l can also be defined in terms of a screening length, with scaled results also lying quite close to a universal relation.[5]

The universal nature of total-energy curves is not limited to metal interfaces or to simple metals. It has been found[7] that bulk cohesive energies as a function of Wigner-Seitz radius scale in exactly the same fashion as do adhesive energies at interfaces. From the two definitions of l [screening length or Eq. (20)], a simple relationship between surface energies and cohesive energies ensues, as described earlier.[7] Furthermore, results for both simple metals and transition metals when scaled [Eq. (20)] fall closely on the universal relation. Finally, many diatomic molecular binding-energy relations, as well as those known for chemisorption and nucleon-nucleon interactions, are also described by the *same* universal relation (Fig. 11). It has been commented earlier about the similarity of the results of Fig. 8 to those of diatomic molecules.[15] We can now see that there is a detailed correspondence between the metallic and molecular bond.[16]

ACKNOWLEDGMENTS

The authors are grateful to Jack Gay, Jim Burkstrand, and Jim Rose for useful discussions, and especially to Jan Herbst for his comments regarding numerical techniques.

[1]John Ferrante and John R. Smith, Phys. Rev. B **19**, 3911 (1979).
[2]D. H. Buckley, J. Colloid Interface Sci. **58**, 36 (1977).
[3]Alan J. Bennett and C. B. Duke, Phys. Rev. **160**, 541 (1967); **162**, 578 (1967).
[4]John Ferrante and John R. Smith, Surf. Sci. **38**, 77 (1973); Solid State Commun. **21**, 1059 (1976).
[5]J. H. Rose, John Ferrante, and John R. Smith, Phys. Rev. Lett. **47**, 675 (1981).
[6]John R. Smith, John Ferrante, and J. H. Rose, Phys. Rev. B **25**, 1419 (1982).
[7]John Ferrante, John R. Smith, and James H. Rose, Phys. Rev. Lett. **50**, 1385 (1983); Phys. Rev. B **28**, 1835 (1983); Phys. Rev. Lett. **53**, 344 (1984).
[8]P. Hohenberg and W. Kohn, Phys. Rev. **136**, B864 (1964).
[9]W. Kohn and L. J. Sham, Phys. Rev. **140**, A1133 (1965).
[10]N. W. Ashcroft, Phys. Rev. **155**, 682 (1967).
[11]J. H. van der Merwe, in *Surfaces and Interfaces*, edited by J. J. Burke *et al.* (Syracuse University Press, Syracuse, 1966), Vol. 1, p. 361.
[12]H. F. Budd and J. Vannimenus, Phys. Rev. Lett. **31**, 1218 (1973).
[13]B. Raykov, Solid State Commun. **25**, 257 (1978).
[14]N. D. Lang and W. Kohn, Phys. Rev. B **1**, 4555 (1970).
[15]M. J. Feinberg and Klaus Ruedenberg, J. Chem. Phys. **54**, 1495 (1971); C. Woodrow Wilson, Jr. and William A. Goddard, III, Theor. Chem. Acta **26**, 195 (1972).
[16]For further discussion of this correspondence, see Ref. 7.